



## Diffusion creep of dry, melt-free olivine

Ulrich H. Faul<sup>1,2</sup> and Ian Jackson<sup>1</sup>

Received 21 June 2006; revised 9 November 2006; accepted 3 January 2007; published 12 April 2007.

[1] Deformation experiments were conducted on fine-grained (3–6  $\mu\text{m}$ ), fully synthetic  $\text{Fo}_{90}$  olivine aggregates in a gas-medium apparatus at 300 MPa confining pressure and temperatures of 1150–1360°C. The strain rates of the solution-gelation-derived and therefore genuinely melt-free, dry samples are about two orders of magnitude lower than the strain rates for nominally melt-free aggregates at the same pressure and temperature conditions and grain size. Benchmark deformation tests with Anita Bay dunite and mild steel reproduce published data. The creep strength of melt-added sol-gel olivine is similar to the published creep strength of dry, melt-bearing olivine derived from natural rocks. Nonlinear least-squares fits to the melt-free deformation data give an activation energy of 484 kJ/mol, a stress exponent of 1.4, and a grain-size exponent of 3 over a range of stresses from 15 to 210 MPa. These results suggest that small amounts of melt may be similarly effective in reducing the creep strength of upper mantle rocks as small amounts of water. However, a possible contribution of grain boundary composition to the observed differences in rheology in the absence of melt cannot be conclusively ruled out by the current experiments.

**Citation:** Faul, U. H., and I. Jackson (2007), Diffusion creep of dry, melt-free olivine, *J. Geophys. Res.*, 112, B04204, doi:10.1029/2006JB004586.

### 1. Introduction

[2] The rheology of melt-free upper mantle rocks has been determined almost exclusively by deformation of polycrystalline samples derived from natural rocks [Chopra and Paterson, 1981; Cooper and Kohlstedt, 1984; Karato *et al.*, 1986; Borch and Green, 1989; Hirth and Kohlstedt, 1995; Bystricky *et al.*, 2000; Mei and Kohlstedt, 2000b]. In these experiments, the precursor material was either cored directly from a boulder [e.g., Chopra and Paterson, 1981] or the individual olivine grains were handpicked, ground, and isostatically hot pressed to obtain sufficiently fine grained material for deformation in the diffusion creep regime at laboratory strain rates.

[3] In order to determine the effect of melt on the deformation behavior, small amounts of basaltic melt were added to the reconstituted natural starting material [Cooper and Kohlstedt, 1984; Hirth and Kohlstedt, 1995]. The additional amount of melt was found to enhance creep rates only moderately at melt contents below  $\sim 5\%$  and led to the conclusion that the presence of melt, for example, beneath mid-ocean ridges, has only a minor effect on the rheology of upper mantle rocks [Hirth and Kohlstedt, 1995]. When the effect of dehydration of olivine at the onset of melting is taken into account, melting followed by melt extraction is

predicted to increase the viscosity of the residue [Karato *et al.*, 1986; Hirth and Kohlstedt, 1996].

[4] However, Hirth and Kohlstedt [1995] [see also Mei and Kohlstedt, 2000b] pointed out that the reference material for melt-free behavior (to which no melt was deliberately added) was only nominally melt-free and actually contained up to 1% melt. The presence of  $<0.1$ –1% melt was also reported in the reconstituted samples deformed by Karato *et al.* [1986, p. 8165].

[5] High resolution of stress and strain rates during experimental deformation of rocks at the relatively small differential stresses in the diffusion creep regime necessitates the use of a gas-medium apparatus. This limits the pressure range of the experiments, which are typically conducted at 300 MPa and at temperatures from 1200 to 1300°C. By comparison, the solidus even of depleted peridotite at this pressure is below 1200°C [e.g., Green and Falloon, 1998].

[6] Natural rocks such as xenoliths and dunites from ophiolites generally contain not only spinel and pyroxenes but also hydrous accessory phases like amphibole, as well as glass and secondary alteration phases such as serpentine and talc [Frey and Prinz, 1978; Chopra and Paterson, 1981; Wirth, 1996]. Samples cored from natural rocks therefore invariably contain melt at experimental conditions (Figure 1) [Fitz Gerald and Chopra, 1982; Chopra and Paterson, 1984]. Even for handpicked olivine grains, it is practically impossible to exclude all glass attached to grain boundaries or spinel and glass inclusions inside olivine grains for the tens of grams that are required for a series of experiments.

[7] In contrast to the reported minor effect of melt on moderate-strain compressive deformation behavior, measurements of seismic properties on pure, synthetic, and

<sup>1</sup>Research School of Earth Sciences, The Australian National University, Canberra, Australia.

<sup>2</sup>Now at Department of Earth Sciences, Boston University, Boston, Massachusetts, USA.

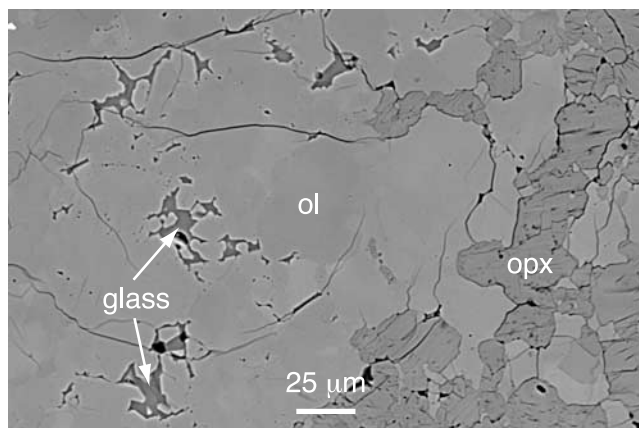


**Figure 1.** Scanning electron microscope (SEM) back-scattered electron (BSE) image of Anita Bay dunite after deformation at 1200°C. The abbreviations “ol” and “opx” denote olivine and orthopyroxene, respectively. The as-received rock has a heterogeneous distribution of pyroxene, spinel, and hydrous accessory phases. Correspondingly, the melt content varies considerably, from not detectable by SEM imaging up to 10% locally. The melt pockets (now quenched to glass) tend to be surrounded by smaller-than-average olivine grains. Cracks are due to the relatively rapid drop in temperature at the end of the deformation experiment (~100°C in the first minute).

therefore genuinely melt-free polycrystalline olivine indicate that even melt contents as low as 0.01% result in an observable effect on mechanical properties [Jackson *et al.*, 2004; Faul *et al.*, 2004]. Grain-scale processes such as diffusion and grain boundary sliding, which are responsible for the viscoelastic behavior in microstrain forced oscillation tests, also contribute to the much larger strains produced during conventional large-strain deformation experiments, and ultimately to deformation and convective flow in the upper mantle, although the rate-limiting step during deformation may be different.

[8] The aim of this study is therefore to determine the creep strength of genuinely melt-free olivine aggregates by using fully synthetic starting materials. The effect of melt can then be verified by deliberately adding small amounts of basaltic glass to the starting material. Consistent with the seismic property measurements on the same class of materials, the experiments presented here show that even small amounts of melt substantially enhance strain rates relative to genuinely melt-free materials. Benchmark deformation experiments on dunite samples cored from the same boulder as those by Chopra and Paterson [1981], as well as deformation of mild steel, verify that the observed behavior is due to differences in the sample materials used and not an artifact of the particular deformation apparatus or testing protocol.

## 2. Sample Materials

[9] Four different types of materials were deformed in this study: fully synthetic, solution-gelation-derived olivine, both melt-free and melt-added; cored dunite samples; and plugs of mild steel. Experiments with the latter material also served to determine the correction of the observed deformation behavior for the strength of the mild steel jackets.

[10] For the deformation experiments on natural dunite, the same boulder of hand-specimen size from Anita Bay, New Zealand, used for the study by Chopra and Paterson [1981] was similarly cored perpendicular to the foliation. The plugs were precision-ground and jacketed for deformation without prior heat treatment. As described by Chopra and Paterson, Anita Bay dunite contains locally abundant spinel and alteration phases such as talc and serpentine. The average olivine grain size is about 100  $\mu\text{m}$ , although, locally, the areas of much more fine grained material were observed, as well as porphyroclasts of up to several millimeters in size. Orthopyroxene (opx) grains range from tens of micrometers up to millimeters in size.

[11] The manufacture of the solution-gelation-derived olivine is described in the studies of Jackson *et al.* [2002] and Faul and Scott [2006]. The sequence of steps from

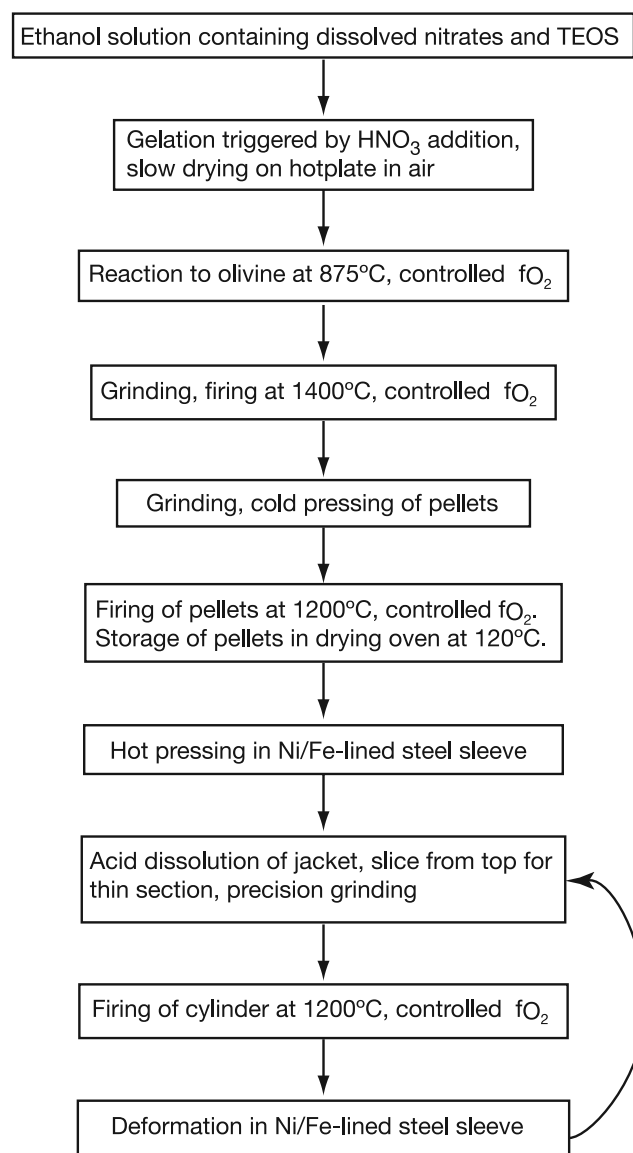


**Figure 2.** Flowchart showing the steps during sample manufacture and deformation, including repeated firing at high temperature and controlled oxygen atmosphere to ensure that the samples remained dry.

solution gelation to deformation is shown in Figure 2. Briefly, Fe and Mg nitrates were dissolved in ethanol, to which tetraethyl orthosilicate was added. The gel resulting from the addition of a small amount of nitric acid was dried at successively higher temperatures and finally reacted to olivine of composition  $(\text{Fe}_{0.1}\text{Mg}_{0.9})_2\text{SiO}_4$  in a controlled oxygen atmosphere at  $1400^\circ\text{C}$  and  $f_{\text{O}_2} \sim 10^{-8}$ – $10^{-9}$  atm. The resulting plugs were highly porous with a grain size  $<1 \mu\text{m}$ . The plugs were reground and refired before hot pressing at 300 MPa for 20–24 hours in Fe jackets. Before insertion of the samples into the jackets, they were completely surrounded by  $\text{Fe}_{30}\text{Ni}_{70}$  foil. The silica activity of the samples was buffered by opx, resulting from the addition of an amount of silica slightly in excess of that required for stoichiometric olivine.

[12] After hot pressing, the samples were recovered by dissolution of the jackets and liners in nitric acid, and a 1-mm-thick slice was cut off from the upper end for microstructural examination. After precision grinding, the density was checked by the Archimedeian method involving immersion in ethanol. After firing at  $1200^\circ\text{C}$  at  $f_{\text{O}_2} \sim 10^{-9}$  atm, the samples were inserted in  $\text{Fe}_{30}\text{Ni}_{70}$ -lined Fe jackets for deformation. Sample dimensions and experimental details are given in Table 1. Where indicated, a few samples were further deformed after a 1-mm-thick slice was cut off for microstructural examination, regrinding, and firing.

[13] The firing of the samples in a controlled oxygen atmosphere furnace before each jacketed high-pressure experiment (hot pressing or deformation, see Figure 2) served to eliminate adsorbed water. Experience shows that any adsorbed water induces abnormal grain growth even at  $1200^\circ\text{C}$  in these pure samples. During abnormal grain growth, some grains grow very rapidly to  $100 \mu\text{m}$  in size. Depending on how much water is initially present and retained in the sample over the course of the experiment, this process may approach completion in 24 hours, where only small pockets of grains with the original size are left.

[14] For melt-added samples, sintered oxide-derived basaltic glass powder was ground together with the sol-gel-derived olivine in an agate mortar. The composition of the added basaltic glass is given in Table 2 of the paper of *Faul et al.* [2004]. The basalt composition was designed to be approximately in equilibrium with a four-phase assemblage (olivine, two pyroxenes, and plagioclase) at 300 MPa and  $\sim 1250^\circ\text{C}$  [*Cmiral et al.*, 1998]. The amount of melt shown in Table 1 (runs 6563 and 6574) was determined by hand tracing of melt pockets on digital backscattered electron (BSE) images of hot-pressed samples.

### 3. Microstructural Characterization

#### 3.1. Imaging and Fourier Transform Infrared Spectroscopy

[15] Scanning electron microscope (SEM) imaging and electron backscatter diffraction (EBSD) mapping show that the olivine grains have regular shapes with near-ideal hexagonal or “foam” textures and gently curved grain boundaries (Figure 3). The five different sol-gel batches from which the samples of the present study were derived contain variable amounts of opx, ranging from 0.1% to 12.3% (Table 1). Most of the opx is concentrated in large

( $>10 \mu\text{m}$ ) grains, or intergrowths of olivine and opx (lower left corner, Figure 3c), although widely distributed grains  $<1 \mu\text{m}$  in size are also present in most batches. While most opx grains occur on olivine grain boundaries, some occur as inclusions in olivine in coarser-grained samples (Figure 3d). Pores also occur on grain boundaries and intragranularly.

[16] In all samples, pores and opx grains are irregularly distributed relative to the network of olivine grain boundaries and grain edges, such that the majority of olivine two-grain boundaries and three-grain edges are free of both pores and opx grains.

[17] Postdeformation examination of the Anita Bay dunite samples shows that melt now quenched to glass was present during deformation at a temperature of  $1200^\circ\text{C}$  (Figure 1). However, this melt is not uniformly distributed throughout the sample but is concentrated presumably at the location of former hydrous phases. Opx and spinel also occur in bands throughout the sample. The spinel shows signs of reaction to plagioclase. In contrast to the heterogeneous melt distribution in the natural dunite, the melt in the melt-added sol-gel samples is homogeneously distributed on a sample scale (Figure 4).

[18] Water contents of representative samples were measured by Fourier transform infrared (FTIR) spectroscopy on doubly polished thick sections. A comparison of the spectra from a deformed Anita Bay dunite sample (6559) with the as-received rock indicates that a significant amount of water was lost over the time of approximately 6 hours at  $1200^\circ\text{C}$ . The spectra from sol-gel samples 6532 and 6542 show that the water content is below the detection limit ( $<10$  ppm) of our spectrometer (Figure 5). In the  $\sim 0.43$ -mm-thick sections used for FTIR spectroscopy, neither sharp peaks corresponding to the stretching frequencies of O-H in olivine nor a broad peak around a wavenumber of  $3400 \text{ cm}^{-1}$  is observable.

#### 3.2. Grain Sizes

[19] Grain sizes were determined by EBSD mapping after hot pressing and after deformation (Figure 6). The maps were collected on a scanning electron microscope with W filament, Nordif camera, and HKL Channel 5 EBSD software. For the most fine grained samples, indexing rates were only about 50%. Comparison of the results from EBSD mapping and determination of grain sizes from transmission electron microscopy (TEM) images shows, however, that the grain sizes are adequately resolved [see *Jackson et al.*, 2002].

[20] Because all but three of the melt-free samples were deformed into the power law creep regime with differential stresses of up to 310 MPa, the final grain sizes of those experiments may have been affected by dynamic recrystallization [e.g., *van der Waal et al.*, 1994]. Grain sizes for the individual segments of constant load for each run were therefore calculated from the grain size measured after hot pressing, with a grain growth equation of the form [e.g., *Atkinson*, 1988]:

$$d^{n_g} - d_0^{n_g} = kt, \quad k = k_0 e^{-E_g/RT} \quad (1)$$

where  $d_0$  is the grain size after hot pressing,  $d$  is the grain size at time  $t$ , and  $k$  is the temperature-dependent rate constant.

**Table 1.** Experimental Conditions and Results<sup>a</sup>

Experiment (Hot-Press)	Material, (% opx)	T, °C	Length <sup>b</sup> , mm	Grain Size <sup>c</sup> , μm	Grain Size <sup>d</sup> , mm	Stress, MPa	Strain Rate, s <sup>-1</sup>	Strain, %						
6436	Mild steel	1000	20.0 <sup>e</sup>			10.8	$6.6 \times 10^{-7}$							
						12.4	$1.9 \times 10^{-6}$							
						16.3	$3.4 \times 10^{-5}$							
						17.8	$1.2 \times 10^{-4}$							
						7.5	$1.6 \times 10^{-5}$							
						7.6	$1.5 \times 10^{-5}$							
						8.0	$4.2 \times 10^{-6}$							
						8.7	$1.1 \times 10^{-5}$							
						9.2	$2.0 \times 10^{-5}$							
						11.0	$1.6 \times 10^{-5}$							
						6502	Mild steel	1000	18.6 <sup>f</sup>			25.3	$2.9 \times 10^{-5}$	
12.3	$2.4 \times 10^{-5}$													
17.3	$1.5 \times 10^{-4}$													
8.7	$3.7 \times 10^{-5}$													
11.8	$1.9 \times 10^{-4}$													
13.0	$5.3 \times 10^{-5}$													
6426	Anita Bay dunite	1200	20.2 <sup>e</sup>		100	43.5	$2.3 \times 10^{-6}$	0.47						
						101	$1.5 \times 10^{-5}$	1.31						
6559	Anita Bay dunite	1200	25.0		100	49.0	$2.1 \times 10^{-6}$	1.24						
						68.4	$3.6 \times 10^{-6}$	2.78						
						96.0	$9.3 \times 10^{-6}$	3.54						
						134	$2.8 \times 10^{-5}$	4.08						
						178	$8.2 \times 10^{-5}$	6.18						
6503 (6500)	Sol-gel (2.6)	1230	20.0 <sup>e</sup>	2.6 3.0	2.74 2.82 2.89 2.96 3.01 3.06 3.09 3.12 3.13	24.5	$1.4 \times 10^{-6}$	0.34						
						24.8	$1.2 \times 10^{-6}$	0.34						
						32.6	$1.6 \times 10^{-6}$	0.46						
						51.9	$2.9 \times 10^{-6}$	0.82						
						68.0	$4.3 \times 10^{-6}$	0.81						
						79.8	$4.8 \times 10^{-6}$	0.92						
						89.2	$5.4 \times 10^{-6}$	1.02						
						104	$6.2 \times 10^{-6}$	0.90						
						135	$9.3 \times 10^{-6}$	0.93						
						6509 (6508)	Sol-gel (2.6)	1300	27.0	5.4 6.8	5.53 5.58 5.62 5.65 5.68 5.71 5.73	28.9	$1.1 \times 10^{-6}$	0.21
59.4	$2.8 \times 10^{-6}$	0.42												
80.5	$4.2 \times 10^{-6}$	0.63												
89.6	$4.8 \times 10^{-6}$	0.45												
104	$5.8 \times 10^{-6}$	0.56												
118	$6.9 \times 10^{-6}$	0.65												
135	$8.7 \times 10^{-6}$	0.51												
6519 (6518)	Sol-gel (6.3)	1300	26.8	4.1 6.5	4.32 4.43 4.50 4.55 4.58	22.7	$2.2 \times 10^{-6}$	0.64						
						43.3	$4.7 \times 10^{-6}$	0.89						
						64.2	$6.8 \times 10^{-6}$	0.95						
						86.4	$9.3 \times 10^{-6}$	0.83						
						106	$1.2 \times 10^{-5}$	0.85						
						126	$1.6 \times 10^{-5}$	0.71						
6523 (6521)	Sol-gel (6.3)	1150	26.0	3.6 4.4	4.02 4.05 4.07 4.09	101	$2.0 \times 10^{-7}$	0.40						
						134	$3.0 \times 10^{-7}$	0.46						
						166	$4.2 \times 10^{-7}$	0.50						
						211	$6.0 \times 10^{-7}$	0.43						
6526 (6522)	Sol-gel (6.3)	1236	21.3	4.2 4.6	4.48 4.52 4.56	81.5	$1.2 \times 10^{-6}$	0.45						
						102	$1.7 \times 10^{-6}$	0.80						
						132	$2.6 \times 10^{-6}$	0.86						
6527 (6523)	Sol-gel (6.3)	1185	21.9	4.4 3.7	4.47 4.54 4.78 4.42 4.62 4.71 4.42	57.9	$2.2 \times 10^{-7}$	0.39						
						77.5	$3.2 \times 10^{-7}$	1.05						
						79.5	$2.5 \times 10^{-7}$	0.75						
						104	$6.1 \times 10^{-7}$	0.26						
						104	$4.2 \times 10^{-7}$	1.05						
						133	$5.9 \times 10^{-7}$	1.05						
						159	$1.3 \times 10^{-6}$	0.63						
						6530 (6525)	Sol-gel (6.3)	1360	23.9	4.0 5.5	4.63 4.25 4.86 4.32 4.98 4.35	14.2	$2.6 \times 10^{-6}$	0.89
												15.2	$3.5 \times 10^{-6}$	0.27
28.7	$6.6 \times 10^{-6}$	1.32												
29.7	$8.4 \times 10^{-6}$	0.34												
60.3	$1.6 \times 10^{-5}$	1.51												
61.1	$2.1 \times 10^{-5}$	0.51												
6532 (6529)	Sol-gel (12.3)	1250	25.3	2.7 4.2	2.93 3.17 3.31 3.39	15.8	$6.8 \times 10^{-7}$	0.67						
						25.9	$9.5 \times 10^{-7}$	0.67						
						41.3	$1.7 \times 10^{-6}$	0.62						
						60.3	$2.9 \times 10^{-6}$	0.83						

Table 1. (continued)

Experiment (Hot-Press)	Material, (% opx)	$T$ , °C	Length <sup>b</sup> , mm	Grain Size <sup>c</sup> , μm	Grain Size <sup>d</sup> , mm	Stress, MPa	Strain Rate, s <sup>-1</sup>	Strain, %	
6534 (6533)	Sol-gel (12.3)	1250	31.3	3.0	3.46	85.6	$4.4 \times 10^{-6}$	1.29	
					3.52	120	$7.0 \times 10^{-6}$	1.67	
					3.25	14.9	$6.9 \times 10^{-7}$	0.62	
					3.45	19.4	$7.8 \times 10^{-7}$	0.62	
					3.59	27.6	$1.1 \times 10^{-6}$	0.65	
					3.68	38.9	$1.6 \times 10^{-6}$	0.62	
					3.75	53.4	$2.3 \times 10^{-6}$	0.69	
					3.80	75.6	$3.7 \times 10^{-6}$	0.92	
6540 (6534)	Sol-gel (12.3)	1300	25.0	3.9	3.81	110 <sup>g</sup>	$6.2 \times 10^{-6}$	1.14	
					4.49	21.8	$8.4 \times 10^{-7}$	0.59	
					4.77	21.6	$1.1 \times 10^{-6}$	1.04	
					5.08	38.8	$2.1 \times 10^{-6}$	0.48	
					5.21	40.1	$2.0 \times 10^{-6}$	0.81	
					5.29	53.8	$2.9 \times 10^{-6}$	0.82	
					5.35	76.0	$4.7 \times 10^{-6}$	1.08	
					5.39	108 <sup>g</sup>	$8.5 \times 10^{-6}$	0.81	
6542 (6536)	Sol-gel (11.1)	1350	25.3	4.1	4.60	17.8	$1.6 \times 10^{-6}$	0.60	
					5.3	4.86	23.7	$2.3 \times 10^{-6}$	0.70
					5.02	30.1	$3.0 \times 10^{-6}$	0.59	
					5.13	42.1	$4.5 \times 10^{-6}$	0.56	
					5.19	56.4	$6.3 \times 10^{-6}$	0.54	
					5.24	74.4	$8.7 \times 10^{-6}$	0.57	
					5.28	96.6 <sup>g</sup>	$1.3 \times 10^{-5}$	0.57	
					2.73	27.9	$1.9 \times 10^{-7}$	0.57	
6583 (6580)	Sol-gel (0.12)	1150	31.0	2.7	2.82	37.4	$2.0 \times 10^{-7}$	0.35	
					3.0	2.89	53.9	$3.3 \times 10^{-7}$	0.43
					2.93	75.6	$4.8 \times 10^{-7}$	0.56	
					2.97	102	$6.7 \times 10^{-7}$	0.60	
					2.99	134	$9.8 \times 10^{-7}$	0.48	
					3.00	181	$1.6 \times 10^{-6}$	0.31	
					52.2	52.2	$2.3 \times 10^{-7}$		
					70.8	70.8	$3.3 \times 10^{-7}$		
6563 (6561)	Sol-gel (0.2% melt)	1300	31.3	30	85.2	85.2	$4.5 \times 10^{-7}$		
					33	70.8	70.8	$3.3 \times 10^{-7}$	
						91.6	91.6	$5.3 \times 10^{-7}$	
						24.8	24.8	$6.0 \times 10^{-6}$	
6574 (6566)	Sol-gel (4% melt)	1300	31.2	10.4	36.8	36.8	$8.6 \times 10^{-6}$		
					14.6	53.7	53.7	$1.7 \times 10^{-5}$	

<sup>a</sup>The pressure for all experiments was 300 MPa. The sample diameter was 11.5 mm unless noted otherwise.

<sup>b</sup>Length of the sample cylinder before deformation.

<sup>c</sup>Grain size measured after hot-pressing (upper entry) and after deformation (lower entry).

<sup>d</sup>Grain size calculated with equation (1) from grain size after hot pressing for half time of each segment, taking into account the time at temperature before the beginning of deformation.

<sup>e</sup>10-mm diameter.

<sup>f</sup>11.1-mm diameter.

<sup>g</sup>Quenched at this stress.

[21] The constant  $k_0$ , the growth exponent  $n_g$ , and the activation energy  $E_g$  were fitted to minimize the difference between the calculated grain size and the grain size measured at the end of each of the experiments which was terminated within the diffusion creep regime. Since there is a trade-off among the three parameters in the calculation of the final grain size, a second consideration was the effect of the grain growth parameters on the minimization of the misfit of the rheological data (see below). The best fitting combination of parameters thus derived is  $n_g = 3.3$ ,  $k_0 = 1 \times 10^{-9} \text{ m}^n \text{ s}^{-1}$ , and  $E_g = 400 \text{ kJ/mol}$ . The grain growth rate for melt-free olivine determined in this study is lower than that in the work of *Nichols and Mackwell* [1991]. A comparison of the growth rate for the melt-free olivine from this study with melt-added sol-gel olivine [*Faul and Scott*, 2006] shows that the presence of melt enhances grain growth.

[22] With the exception of run 6580, the grain sizes after hot pressing are moderately well correlated with opx content, where samples with higher opx content have a smaller

grain size at a given hot-pressing temperature. The grain sizes are also weakly correlated with hot-pressing temperature. Inhomogeneity of the gel before the reaction to olivine likely influences the grain size after hot pressing, causing the scatter in grain sizes.

[23] During relatively rapid drying of the gel, FeO and MgO may have been concentrated in a crust on the walls of the Pt crucible, resulting in the relatively large opx contents. The sol-gel batch for samples 6580/6583 was dried for 24 hours at 200°C on a hot plate after gelation before exposure to higher temperature. It was reacted to olivine at 875°C in a controlled oxygen environment [see, e.g., *McDonnell et al.*, 1999] before regrinding and firing at 1400°C. This modified procedure likely resulted in the lower opx content and smaller grain sizes after hot pressing of the samples derived from this batch.

[24] The grain-size distributions of both hot-pressed and deformed samples are close to grain-size distributions expected for steady state grain growth (Figure 7). Both

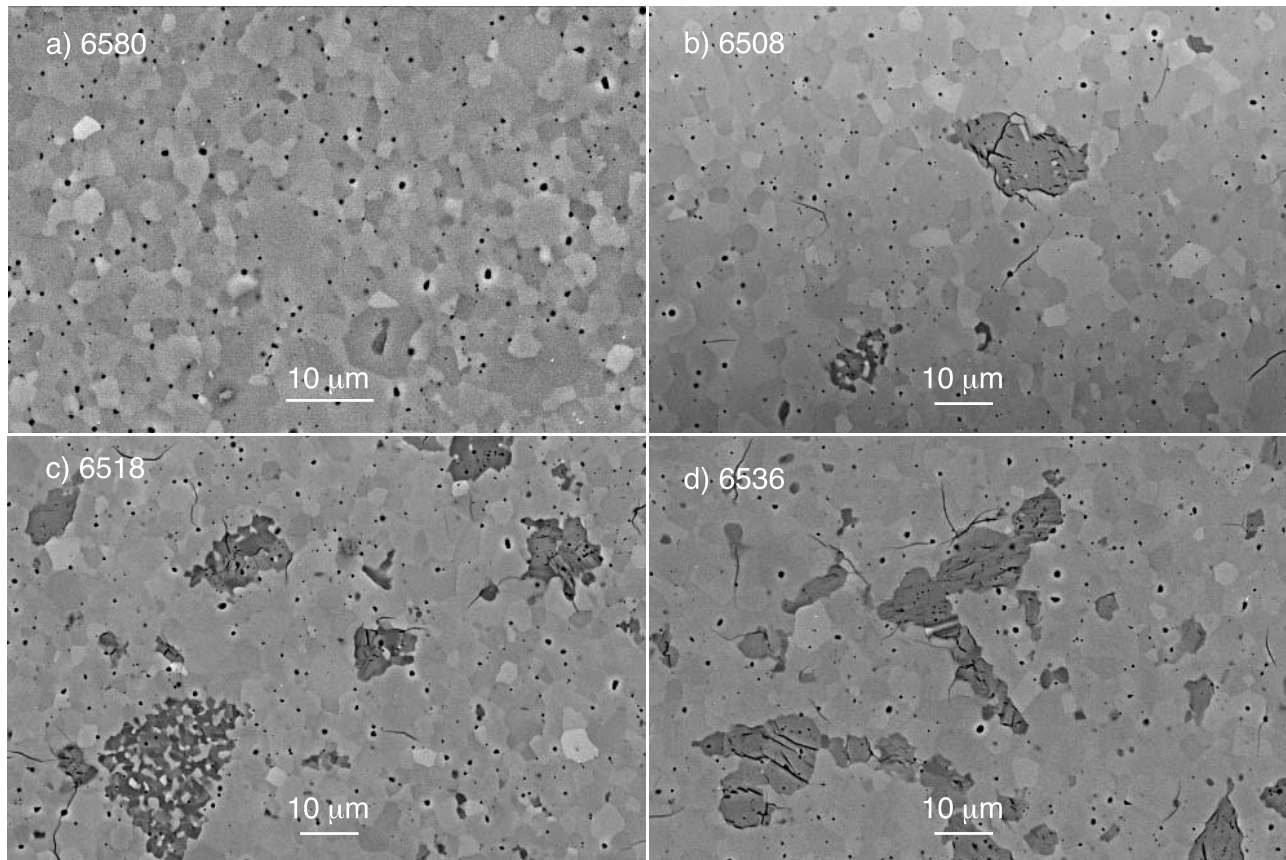


**Figure 3.** SEM-BSE images of representative specimens prepared from four of the different sol-gel batches used in this study. Darker gray grains are orthopyroxene grains, lighter grays are olivine, while black are pores. Olivine grains exhibit orientation contrast even in normal BSE imaging mode (SEM with LaB6 filament) because of the final polish with colloidal silica. Opx occurs as (b–d) clusters of fairly coarse grains, (c) intergrown opx and olivine, and (b–d) dispersed submicron-sized grains. Note the higher magnification in Figure 3a is relative to the three other images.

distributions shown in the figure are statistically indistinguishable from the log-normal distribution.

#### 4. Deformation Experiments and Calibration

[25] The deformation experiments, conducted in a Paterson-type gas-medium apparatus [Paterson, 1990], involve triaxial compression of the samples at a confining pressure of 300 MPa. The load on the sample was monitored by an internal four-element strain gauge load cell, operated as a Wheatstone bridge balanced at zero load. The voltage output from the imbalance of the load cell due to an applied differential stress was converted into kilonewton(s) by calibration against a steel spring of known stiffness. The spring constant was independently determined on an Instron testing apparatus in the Faculty of Engineering and Information Technology at the Australian National University. The apparatus distortion was determined up to 1300°C with a Lucalox<sup>™</sup> alumina (General Electric Lighting) control specimen, which behaves essentially elastically even at this temperature [Jackson, 2000]. All experiments reported in Table 1 were creep tests (Figure 8), where the load was kept constant by servo control of the output of the strain gauge load cell.

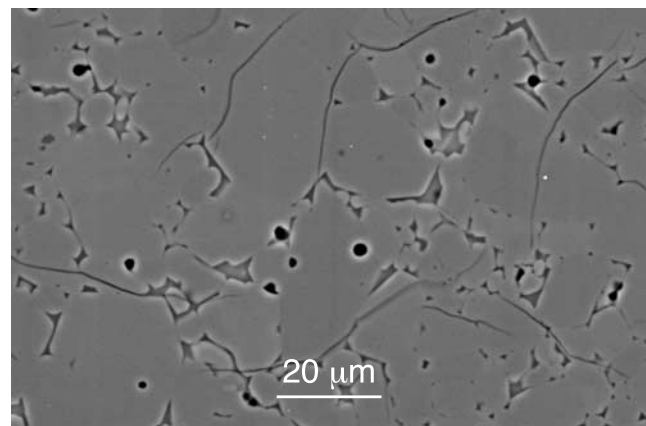


**Figure 4.** SEM-BSE image of the melt-added sample 6566. Instead of many small pores in the melt-free samples, fewer but larger pores are present in the melt-added samples. A melt content of 4 vol.% was determined for this sample from image processing.

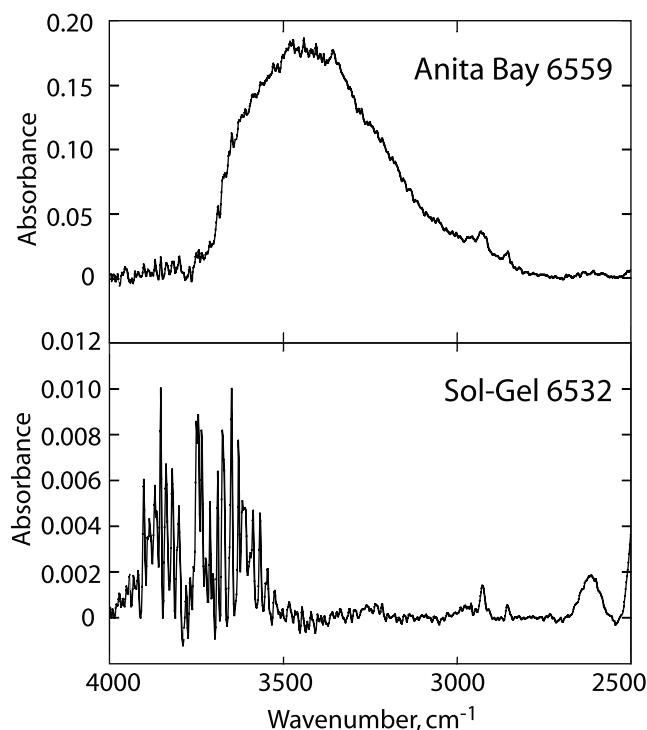


**Figure 5.** FTIR spectrum of an Anita Bay dunite sample after deformation and a representative spectrum of a sol-gel sample after deformation. Note the difference in scale for the absorbance.

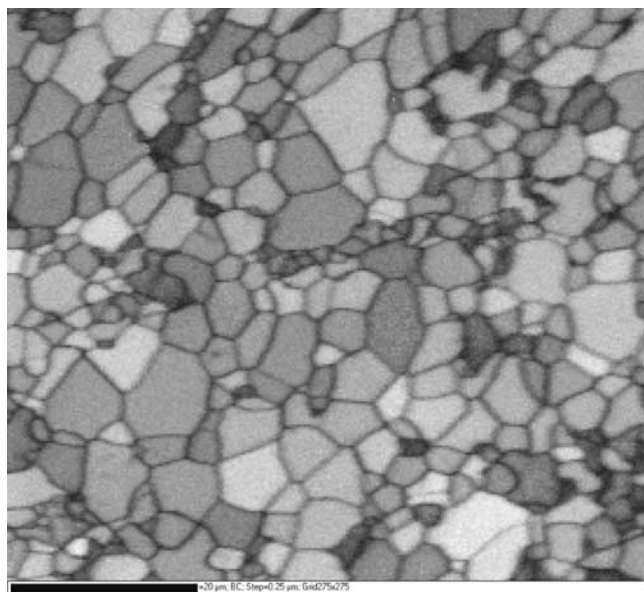


**Figure 6.** EBSD band contrast image of sample 6540 deformed at 1300°C in the diffusion creep regime only. Scale bar at the left bottom represents 20  $\mu\text{m}$ . The grains remain substantially equiaxed during deformation, consistent with the notion that the externally imposed strain is accommodated by diffusively accommodated grain boundary sliding (Ashby and Verrall [1978]; see text).

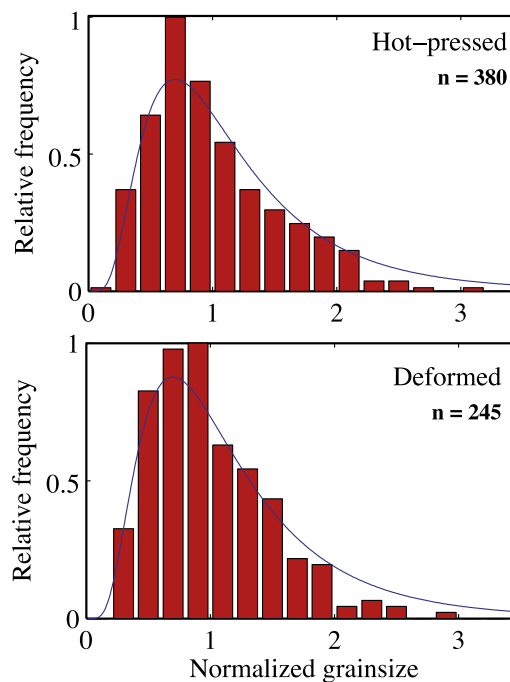


**Figure 7.** Normalized grain-size distributions of hot-pressed sample 6525 and deformed sample 6540 both at 1300°C. The grain sizes and histograms are normalized by the mean and the maximum of the distribution, respectively. The curve indicates a log-normal distribution with the same number of grains. The distributions are narrower than those observed for grain growth in melt-bearing samples [Faul and Scott, 2006].

[26] The temperature was controlled using a Eurotherm controller and a type R Pt-Rh thermocouple. The temperature profile of the three-zone furnace was regularly calibrated to minimize temperature gradients across the sample and to determine the temperature offset at the thermocouple position relative to the sample located in the hot zone. The temperature uncertainty is estimated to be  $\pm 10^\circ\text{C}$ . The pressure was maintained in the range of 295–300 MPa by an automated intensifier.

[27] To check the load cell calibration and jacket corrections, we deformed two samples of mild steel of similar composition as our mild steel jackets. The resulting data are shown in Figure 9 together with the flow law for mild steel given by Frost and Ashby [1982]. Because of the satisfactory agreement of our data with the published flow laws, and the possible minor compositional differences between the deformed mild steel specimen and the jacket material in our experiments, we used the flow law given by Frost and Ashby for the subtraction of the load supported by the jacket. For a description of the microstructures in the mild steel samples, see the paper of Jackson *et al.* [2000].

[28] For a comparison with published deformation data on olivine, we deformed two samples of Anita Bay dunite, cored perpendicular to the foliation and deformed without prior firing as in the study of Chopra and Paterson [1981]. As shown in Figure 10, the agreement with the flow laws of Chopra and Paterson is excellent. The deformation experi-

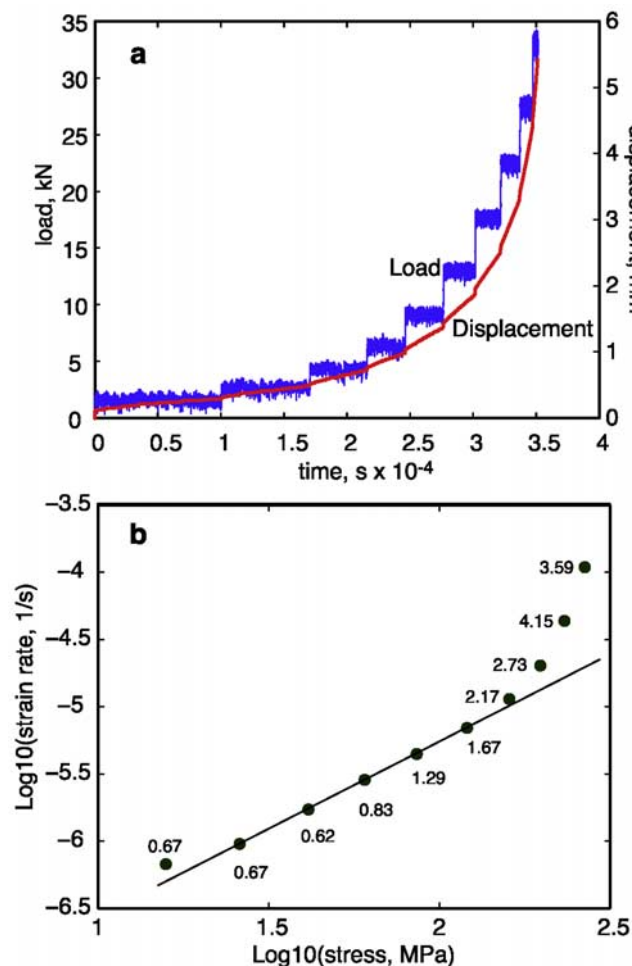


**Figure 8.** (a) Load and displacement history of sample 6532 deformed to a maximum stress of 266 MPa. The load was continuously increased without stepping to zero load before the next higher load segment. The load cell was balanced after reaching the target pressure and temperature and was not observed to drift even after more than 20 hours under a range of loads as long as a constant pressure was maintained. (b) Rheological data showing the transition from near linear to power law creep. Numbers next to data points give the strain (in %) for each constant load segment. The straight line is a fit to segments 2–6 only (starting from the lowest stresses and strain rates). The transition to power law creep can be clearly identified.

ments of Chopra and Paterson were conducted on a different apparatus to that used in this study.

[29] Each sol-gel-derived olivine sample was deformed at one temperature only in a series of constant load creep tests (Figure 8). Deformation at constant temperature reduces the uncertainties in the calculation of the grain size for each deformation segment. Except for runs 6503 and 6509, the series of tests at increasing load was preprogrammed. The samples were quenched under load after the highest stress segment for each sample (Figure 8a).

[30] A total of 12 melt-free sol-gel samples were deformed in diffusion creep at temperatures ranging from 1150 to 1360°C (Table 1). Samples 6534, 6540, and 6542 were

deformed in diffusion creep only, with the maximum stress for each sample given in Table 1. Deformation of the other samples was continued into the power law creep regime. These data will be published separately.

## 5. Results

[31] The creep behavior of rocks is generally described by a flow law of the form:

$$\dot{\epsilon} = A\sigma^n d^{-p} \exp^{-E_d/RT} \quad (2)$$

where  $\dot{\epsilon}$  is the axial strain rate,  $\sigma$  is the differential stress,  $d$  is the grain size,  $A$  is the material-dependent constant,  $E_d$  is the activation energy for creep,  $T$  is the (absolute) temperature,  $n$  is the stress exponent, and  $p$  is the grain-size exponent [e.g., *Frost and Ashby, 1982; Ranalli, 1995*]. The data shown in Table 1 were fitted by a least-squares method to:

$$\ln(\dot{\epsilon}) = \ln(A) + n\ln(\sigma) - p\ln(d) - E_d/RT \quad (3)$$

[32] Figure 11 shows the data and resulting fit. The best fitting parameters are  $A = 2 \pm 4 \times 10^{10} \text{ MPa}^{-n} \text{ s}^{-1} \mu\text{m}^p$ ,  $E_d = 484 \pm 30 \text{ kJ/mol}$ , and  $n = 1.37 \pm 0.06$  with  $p = 3$  fixed. No systematic deviation of the data from the fit is observable for the parameters included in the fit over the full range in grain size (2.7–5.7  $\mu\text{m}$ ) and temperature (1150–1360°C; Figure 12). Particularly no deviation from  $n = 1.37$  is observable for stresses from 14 to 211 MPa. The uncertainties were derived from fits where individual runs with a relatively large misfit (for example, 6542) were removed, as well as from fits where the grain growth parameters were varied.

[33] As already evident in Figure 11, run 6542 has the largest deviation from the fit with the measured strain rate lower than expected for the grain size and temperature. A

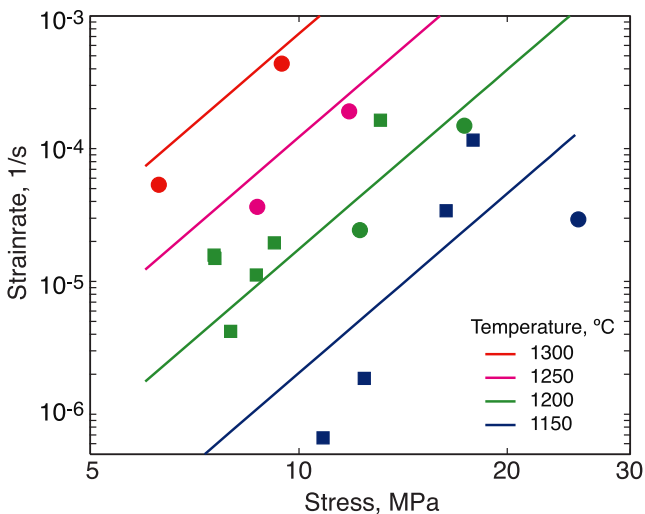


**Figure 9.** Comparison of the rheology of mild steel from this study (symbols) with the flow law published by *Frost and Ashby* [1982]. While there is some scatter in the data, there is no systematic difference between the published flow law and our measurements. Square symbols indicate run 6436, whereas round symbols show run 6502.

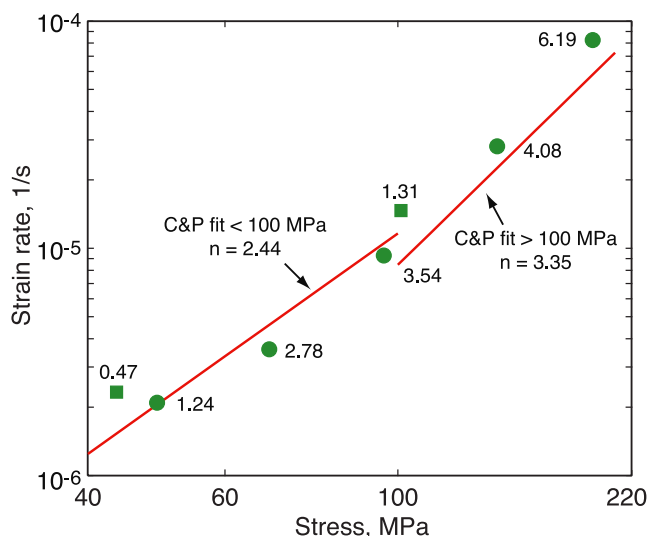


**Figure 10.** Comparison of the rheology of unfired Anita Bay dunite at 1200°C. Solid lines are the flow laws determined by *Chopra and Paterson* [1981]. Square and round symbols indicate runs 6426 (no liner; sample is in direct contact with the Fe jacket) and 6559 (Fe<sub>30</sub>Ni<sub>70</sub> liner), respectively. The numbers indicate the strain (in %) at each constant load segment. The two experiments show no resolvable difference in strength even at low stress despite the nominal buffering at a different oxygen fugacity, consistent with the observations of *Chopra and Paterson* [1981].

possible explanation could be that the furnace characteristics during the deformation experiment were different to those during the temperature calibration experiment, resulting in a somewhat lower than expected sample temperature. Temperature calibration after run 6503 showed somewhat different furnace characteristics, so that the temperature for this run had to be corrected.

[34] When both grain size and stress exponent are fixed at values of 3 and 1, respectively, the data systematically deviate from the fit (Figure 13), resulting in a significantly larger residual misfit. The same is the case when only the stress exponent is fixed at  $n = 1$  and  $p$  is allowed to vary. Allowing both  $p$  and  $n$  to vary results in only a relatively minor decrease of the residual misfit relative to  $p = 3$  fixed. Since  $p$  is sensitive to the grain growth parameters, which this study was not designed to constrain, the fit with  $p$  fixed is the preferred fit. Within the uncertainties, the combination of  $n \sim 1.4$  and  $p \sim 3$  is well constrained by the data (Figure 12).

[35] The transition from diffusion to power law creep depends on temperature and ranges from just above 200 MPa at 1150°C to 120 MPa at 1350°C for the grain sizes of this study. As indicated by a comparison of the data and fit in Figure 12a, removing data with stresses above 100 MPa from the fit will not change the resulting stress exponent.

## 6. Comparison With Other Studies

[36] Diffusion creep data at a confining pressure of 300 MPa for dry, nominally melt-free olivine have been

published by *Karato et al.* [1986], *Beeman and Kohlstedt* [1993], *Hirth and Kohlstedt* [1995], and *Mei and Kohlstedt* [2000a, 2000b]. Except for a few experiments of Beeman and Kohlstedt, all studies used handpicked and ground San Carlos olivine as precursor material. In all studies, the samples were hot pressed and the hot-pressing jacket was dissolved in acid prior to reshaping for deformation. Following acid dissolution and reshaping, the heat treatment of the samples prior to deformation differs among the studies. The samples of *Karato et al.* and some of the (partially molten) samples of *Zimmerman and Kohlstedt* [2004] were fired at 1200°C at a controlled oxygen fugacity, as is done in the present study. *Hirth and Kohlstedt* dried their samples at 150°C, *Beeman and Kohlstedt* stored their samples in a desiccator, and *Mei and Kohlstedt* [2000a, 2000b] did not specify a treatment of their “dry” samples.

[37] The most straightforward comparison of the creep data from different studies is done without recalculation to common stress or temperature since the published stress exponents and activation energies differ. However, the published data do need to be recalculated to a common grain size, as grain sizes range from  $\sim 7$  to 18  $\mu\text{m}$  in the studies of *Karato et al.* [1986], *Hirth and Kohlstedt* [1995], and *Mei and Kohlstedt* [2000a, 2000b], while those of *Beeman and Kohlstedt* [1993] and this study range from  $\sim 2$  to 6  $\mu\text{m}$ . *Hirth and Kohlstedt* and *Mei and Kohlstedt* [2000a, 2000b] determined a grain-size exponent  $p \sim 3$  as in this study, while *Karato et al.* reported  $p \sim 2$  for their dry

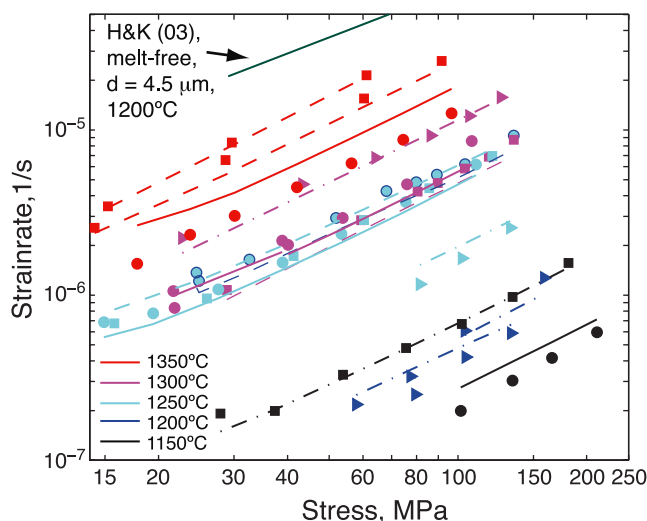


**Figure 11.** Creep data (symbols) and fit (lines) to the melt-free sol-gel samples at temperatures between 1150 and 1360°C. The stress ranges from 14 to 211 MPa, the strain rates from  $2 \times 10^{-7} \text{ s}^{-1}$  to  $2.6 \times 10^{-5} \text{ s}^{-1}$ , while the grain sizes range from 2.7 to 5.7  $\mu\text{m}$ . The lines were calculated from the fit to the data and include the grain-size increase during the experiments. Shown for comparison are the strain rates calculated with the parameters given by *Hirth and Kohlstedt* [2003] for 1200°C (line near the top of figure) for the same (average) grain size as the 1200°C experiment in this study with some of the lowest strain rates measured (dash-dotted line and triangles near the bottom of the figure). The colors are indicative for temperatures in 50° increments only; the exact temperatures are given in Table 1.

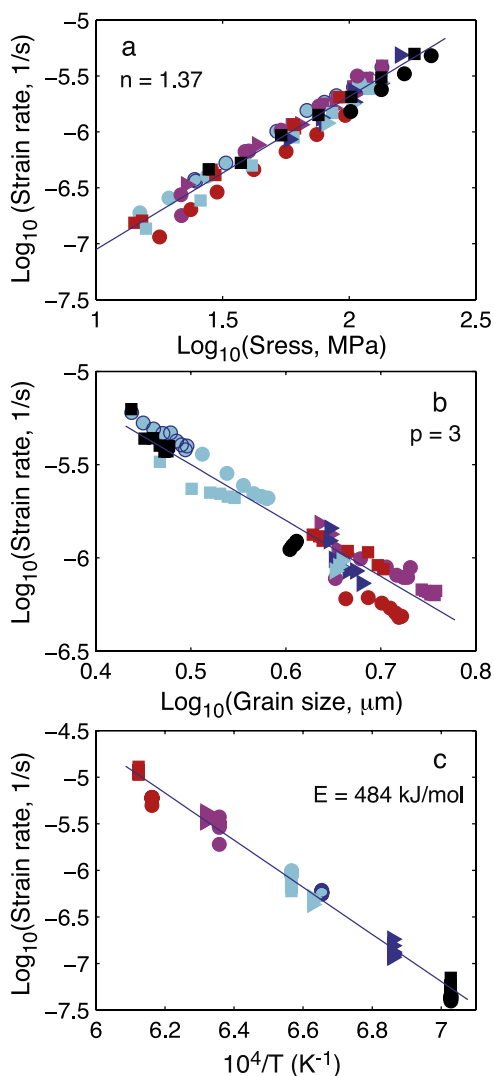


**Figure 12.** Quality of the fit of the data in Table 1 to equation (3). (a) Data were normalized to a common temperature (1250°C) and grain size (5  $\mu\text{m}$ ). The data show no systematic deviation from the fit (solid line) over the whole range of stresses from 14 to 211 MPa, indicating that the exponent is not biased by a transition to power law creep. (b) Data were normalized to a common stress (50 MPa) and a common temperature (1250°C). No systematic deviation of the fit at large or small grain sizes is observable, indicating that the grain-size exponent is well constrained over the range of grain sizes in this study. (c) Data are normalized to a common grain size and stress, showing that the activation energy is well constrained over the relatively large 210°C temperature range of the experiments.

samples. For the comparison of the data below,  $p = 3$  was used.

[38] The grain sizes for the individual stress segments of the study of *Mei and Kohlstedt* [2000a, 2000b] need to be calculated from the initial grain sizes, strains, strain rates (to calculate the elapsed time for each stress segment), and grain growth parameters [*Mei and Kohlstedt*, 2000a, 2000b, Table 1]. The final grain sizes calculated for the dry experiments PI-181, PI-220, and PI-567 with their grain

growth constant  $k_0 = 3.8 \times 10^{-9} \text{ m}^2 \text{ s}^{-1}$  [see equation (1)] were larger than the final grain sizes given by *Mei and Kohlstedt* [2000b]. In order for the final calculated grain size not to exceed the measured grain size given in Table 1 of *Mei and Kohlstedt* [2000a], we decreased the constant  $k_0$  to  $2.2 \times 10^{-9} \text{ m}^2 \text{ s}^{-1}$ . The reason for doing so is that grain growth rates are enhanced by the presence of water [*Karato*, 1989] but *Mei and Kohlstedt* [2000a] did not mention different growth parameters for dry versus wet samples. The growth constant given by *Mei and Kohlstedt* [2000a] appears to apply to the wet samples only. The grain sizes calculated with the somewhat smaller growth constant thus fall between the initial and final grain sizes given by *Mei and Kohlstedt* [2000b].

[39] Figure 14 shows a comparison of creep rates of nominally melt-free olivine with genuinely melt-free olivine. The strain rates determined in this study for genuinely melt-free samples at given temperature, grain size, and stress are about two orders of magnitude lower than the strain rates published by *Hirth and Kohlstedt* [1995] and *Mei and Kohlstedt* [2000a]. This contrast in strength is equivalent to the effect of a temperature difference of more than 200°C (Figure 11). The 1300°C strain rates in the study of *Karato et al.* [1986], again normalized to the same grain size, are similar to the 1250°C data of *Hirth and Kohlstedt* and *Mei and Kohlstedt* [2000a, 2000b] and are a little over

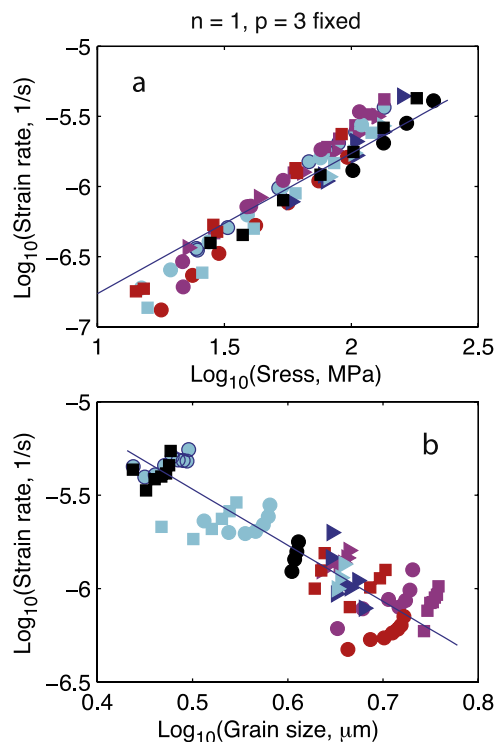


**Figure 13.** Quality of the fit of the data in Table 1 to equation (3) with grain-size exponent and stress exponent fixed at 3 and 1, respectively. The data are again normalized to (a) common temperature and grain size and (b) common stress and temperature. Comparison with Figure 12 emphasizes the systematic misfit in Figure 13a and the much larger scatter in Figure 13b. Fixing  $n = 1$  and allowing  $p$  to vary produce similar misfits.

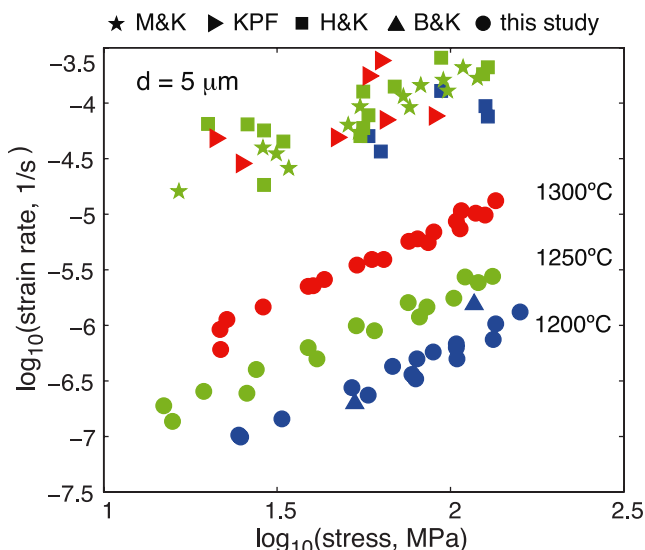


**Figure 14.** Comparison of the creep data for nominally melt-free samples derived from San Carlos olivine and genuinely melt-free sol-gel-derived olivine for experiments conducted at the same temperature. The data are normalized to a common grain size of  $5 \mu\text{m}$  with an exponent  $p = 3$  in equation (2). The colors indicate nominal temperature (blue:  $1200^\circ\text{C}$ , green:  $1250^\circ\text{C}$ , and red:  $1300^\circ\text{C}$ ). The data of *Mei and Kohlstedt* [2000a, 2000b] (MK) and *Hirth and Kohlstedt* [1995] (HK) are systematically offset by about two orders of magnitude in strain rate for a given stress relative to the data from this study. The data of *Karato et al.* [1986] (KPF) are offset by a little more than one order of magnitude and overlap with the data at a  $50^\circ\text{C}$  lower temperature of *Mei and Kohlstedt* [2000a, 2000b] and *Hirth and Kohlstedt*. Note the similarity of the slope of the data from *Mei and Kohlstedt* [2000a, 2000b], with grain sizes recalculated to fit their reported final grain size, and this study, indicating a similar stress exponent. The data from *Beeman and Kohlstedt* [1993] (BK, their runs 7 and 14) are broadly consistent with this study.

one order-of-magnitude higher than the strain rates from this study. The only published high-pressure data, with strain rates for the same conditions comparable to the present study, are those of *Beeman and Kohlstedt* [1993] for fully synthetic and San Carlos olivine-derived samples. As the experiments with mild steel (Figure 9) and Anita Bay dunite (Figure 10), as well as the magnitude of the scatter in Figure 14, show, systematic differences in strain rate greater than a few tenths of a log unit are well outside likely experimental uncertainties.

[40] In order to verify the effect of melt on the creep strength of olivine, two melt-added, solution-gelation-derived samples have also been deformed. To facilitate the comparison of the creep behavior of melt-bearing samples, recalculation of the strain rates to a common melt content is necessary. This is done by multiplying the strain rate given by equation (2) by a factor  $\exp(\alpha\phi)$ , where  $\phi$  is the melt fraction and  $\alpha = 30$  for diffusion creep [*Hirth and Kohlstedt*, 2003]. Since this melt enhancement factor of *Hirth and Kohlstedt* [2003] is derived relative to nominally melt-free

samples containing  $\leq 1\%$  melt, the samples from the study of *Karato et al.* [1986], as well as sample 6563 from this study with actual melt contents  $< 1\%$ , are treated as nominally melt-free for the comparison.

[41] Figure 15 shows data from melt-bearing samples at  $1300^\circ\text{C}$ . For melt-added samples from this study, the difference in strain rates relative to the fit by *Hirth and Kohlstedt* [2003] is reduced to about half an order of magnitude. The data from *Karato et al.* [1986] (also shown in Figure 14) is consistent with our data, while the partially molten lherzolite deformed by *Zimmerman and Kohlstedt* [2004] is marginally weaker.

[42] Relative to the difference in strength between genuinely melt-free aggregates and nominally melt-free aggregates, the decrease in flow strength due to the addition of opx is expected to be relatively small at the opx contents of the present experiments [*McDonnell et al.*, 1999; *Ji et al.*, 2001]. As discussed below, the addition of melt affects every three-grain edge, while opx is much less regularly distributed, and most three-grain edges and two-grain boundaries are opx-free. *Ji et al.* [2001] determined a similar activation energy and stress exponent to this study in their 1-atm deformation experiments on  $\text{Fo}_{100}$ .

## 7. Discussion

### 7.1. Effects of Melt and Water on Creep Rates

[43] As described above, differences in the reported experiments range from the sample material used to the type of metal surrounding the sample and treatment of the samples prior to deformation. *Hirth and Kohlstedt* [1995] attributed the lower strain rates determined by *Karato et al.*

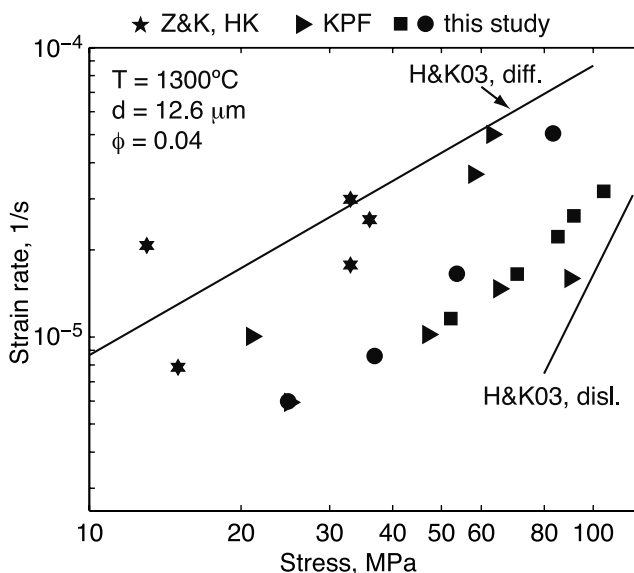


**Figure 15.** Comparison of creep data for melt-bearing samples at  $1300^\circ\text{C}$ . All data are normalized to common grain size [ $12.6 \mu\text{m}$ ; intermediate between the hot-pressed and final grain size of sample 6574 (circles)] and melt content (4%; see text). Solid lines are strain rates calculated for diffusion and dislocation creep with the parameters given by *Hirth and Kohlstedt* [2003]. ZK denotes data from *Zimmerman and Kohlstedt* [2004].

[1986] to the lower oxygen fugacity of their experiments in Fe jackets relative to those of Hirth and Kohlstedt in Ni-lined jackets. However, differences in oxygen fugacity cannot explain the data from this study, as the oxygen fugacity in the present experiments (the samples are surrounded by Fe<sub>30</sub>Ni<sub>70</sub> foil) is intermediate between that of Karato et al. and Hirth and Kohlstedt, but the strain rates are lower than both. *Chopra and Paterson* [1981] as well as we in our deformation experiments with Anita Bay dunite (Figure 10) did not observe any oxygen fugacity dependence in the low stress ( $n = 2.4$ ) regime for different jacket materials.

[44] Another difference between the experimental studies is the heat treatment between hot-pressing and deformation experiments. In all studies, the jackets were dissolved in acid and the samples were ground to cylindrical shape. It is possible that this process introduced adsorbed water on the surface and in cracks in the sample, which can only be eliminated by firing at high temperature. In this study, as well as in those of *Karato et al.* [1986] and *Hirth and Kohlstedt* [1995], the samples were fired above 1000°C at controlled oxygen fugacity prior to deformation, while *Hirth and Kohlstedt* [1995] and *Mei and Kohlstedt* [2000a, 2000b] only oven-dried their samples.

[45] *Hirth and Kohlstedt* [1995], *Mei and Kohlstedt* [2000a], and *Karato et al.* [1986] all described the presence of melt in their experiments. The important aspect of the presence of melt versus a solid phase like opx with respect to the mechanical properties of a polycrystalline sample is the surface energy-controlled distribution of melt at every three-grain edge intersection, even at melt contents of 0.01% (see the TEM observations in the study of *Faul et al.* [2004]). This interconnected melt network provides short-circuit diffusion pathways locally at grain corners as well as on a grain scale. In contrast to partially molten plagioclase aggregates [*Dimanov et al.*, 2000], no melt films >1 nm are observed in partially molten olivine aggregates [*Faul et al.*, 2004].

[46] Additionally, the presence of melt relaxes the space-filling constraints imposed on crystalline grains in subsolidus aggregates. In the model of diffusively accommodated grain boundary sliding, *Ashby and Verrall* [1978] suggested that during neighbor switching, some temporary four-grain edges are created with 90° angles, instead of the ideal three-grain edges with 120° angles of an aggregate with uniformly sized, hexagonal grains.

[47] Starting from melt-free or dry aggregates, the addition of small amounts of melt or water may have a much more pronounced effect on the rheological properties than the addition of the same amount of fluid to an already partially molten or wet aggregate. This proportionally very large effect of the initial fluid addition is suggested by the observed steep increase in height of the attenuation peak by *Jackson et al.* [2004, Figure 10] for melt contents below ~1%. At larger melt contents, the increase in peak height levels off substantially. The effect of melt on the strength of partially molten samples may be similar, so that at melt contents >1%, the rheology for melt-bearing aggregates summarized by *Hirth and Kohlstedt* [2003] is approached.

[48] San Carlos and sol-gel olivine samples differ systematically in the abundance of trace elements such as Ca, Al, and Ti in grain interiors and grain boundaries. These trace elements are enriched in grain boundaries relative to grain interiors, but the abundances in the grain boundaries are correlated with the trace element contents in the grain interiors. While the grain boundary composition differs between San Carlos and sol-gel olivine, high-resolution TEM images of grain boundaries show no difference in their grain boundary structure or any contrast in grain boundary structure between melt-free and melt-bearing polycrystals [*Faul et al.*, 2004]. In order to assess the possible role of grain boundary composition on the deformation behavior of olivine in the absence of melt, further experiments with carefully controlled bulk composition are necessary.

## 7.2. Deformation Mechanisms

[49] Theoretical treatments of deformation in polycrystalline solids predict specific values for the exponents  $n$  and  $p$ . For example, a stress exponent of  $n = 1$  is predicted where grain boundary sliding is accommodated by diffusional processes (diffusional creep). A grain-size exponent  $p = 3$  is predicted for diffusional creep where the dominant diffusion path is along the grain boundaries [*Coble*, 1963; see also *Zimmerman and Kohlstedt*, 2004].

[50] As emphasized by a number of authors, large strains can only be accommodated by coupled diffusional transport of matter and grain boundary sliding [e.g., *Ashby and Verrall*, 1978; *Poirier*, 1985; *Ranalli*, 1995]. The reasoning is that pure Coble or Nabarro-Herring creep without grain boundary sliding would predict that individual grains change their shape in exactly the same way as the imposed macroscopic shape change; that is, for pure shear deformation, the grains would become elongated. Microstructural observations on deformed materials show, however, that the grains remain essentially equiaxed. This is also the case for the experiments in this study, where no systematic shape change is observable (Figure 6).

[51] The value of the grain-size exponent determined in this study ( $p \sim 3$ ) indicates that the dominant diffusion mechanism is grain boundary diffusion, as for nominally melt-free aggregates. The value of the stress exponent is larger than that predicted for diffusively accommodated grain boundary sliding. Preliminary TEM observations from sample 6534, which was deformed at a maximum stress of 106 MPa, show that a few grains have high dislocation densities, similar to the majority of grains from samples deformed well into the power law creep regime at a maximum stress of >250 MPa. This suggests that at least in some grains, part of the imposed deformation is accommodated by dislocations. The nominally melt-free, dry data of *Mei and Kohlstedt* [2000a] recalculated for the increasing grain size during their experiments are also best fit by a stress exponent of ~1.4 (see Figure 14), as found in this study and similar to the observations by *Karato et al.* [1986], although a value of  $1.0 \pm 0.1$  was reported by *Hirth and Kohlstedt* [1995].

[52] The activation energy for diffusion creep is substantially higher than that observed for grain boundary diffusion of Mg and Si (~200 kJ/mol [*Farver and Yund*, 2000]), which are the species with the slowest grain boundary

diffusion in olivine. The large difference in activation energy, together with the larger than expected stress exponent, suggests that deformation is not solely controlled by a diffusive process.

### 7.3. Deformation and Grain Growth

[53] Grain growth rates are significantly enhanced by the presence of water, as noted above and discussed by Karato *et al.* [1986]. Grain growth to 1-mm size in wet conditions takes about 1 year at 1200°C [Karato *et al.*, 1986], whereas in dry conditions, the required time is of the order of tens of millions of years [Nichols and Mackwell, 1991; Faul and Scott, 2006; this study]. More rapid grain growth with on average larger grain sizes in “damp” regions of the upper mantle may mean that they are not much weaker than dry regions with smaller grain sizes. Additionally, because of the larger grain sizes, damp regions may be more likely to deform in dislocation creep [e.g., Drury and Fitz Gerald, 1998].

## 8. Conclusions

[54] The main result from this study is the observation that even small amounts of melt ( $\leq 1\%$ ) have a substantial effect on the rheology of olivine. At least for dry upper mantle, the onset of melting can therefore reduce the creep strength by more than one order of magnitude. Since there are no data on the effect of water on the rheology of genuinely melt-free olivine, the relative effects of melt and water are somewhat difficult to evaluate from published data.

[55] The results from this study also show that the stress exponent for diffusion-dominated creep of dry, melt-free olivine is 1.4 and therefore greater than the theoretically predicted value of 1. Examination of published creep data suggests that this larger exponent also applies, at least at small melt fractions, in partially molten regions of the upper mantle.

[56] **Acknowledgments.** We would like to thank Craig Saint and Harri Kokkonen for their assistance with the deformation experiments and sample preparation. We are also grateful for the constructive reviews by Greg Hirth and Alexandre Dimanov.

## References

- Ashby, M. F., and R. A. Verrall (1978), Micromechanisms of flow and fracture, and their relevance to the rheology of the upper mantle, *Philos. Trans. R. Soc. London, Ser. A*, *A288*, 59–95.
- Atkinson, H. V. (1988), Theories of normal grain growth in pure single phase systems, *Acta Metall.*, *36*, 469–491.
- Beeman, M. L., and D. L. Kohlstedt (1993), Deformation of olivine-melt aggregates at high temperature and confining pressures, *J. Geophys. Res.*, *98*, 6443–6452.
- Borch, R. S., and H. W. Green (1989), Deformation of peridotite at high pressure in a new molten salt cell: Comparison of traditional and homologous temperature treatments, *Phys. Earth Planet. Inter.*, *55*, 269–276.
- Bystricky, M., K. Kunze, L. Burlini, and J.-P. Burg (2000), High shear strain of olivine aggregates: Rheological and seismic consequences, *Science*, *290*, 1564–1567.
- Chopra, P. N., and M. S. Paterson (1981), The experimental deformation of dunite, *Tectonophysics*, *78*, 453–473.
- Chopra, P. N., and M. S. Paterson (1984), The role of water in the deformation of dunite, *J. Geophys. Res.*, *89*, 7861–7876.
- Cmíral, M., J. D. Fitz Gerald, U. H. Faul, and D. H. Green (1998), A close look at dihedral angles and melt geometry in olivine-basalt aggregates: A TEM study, *Contrib. Mineral. Petrol.*, *130*, 336–345.
- Coble, R. L. (1963), A model for boundary diffusion controlled creep in polycrystalline materials, *J. Appl. Phys.*, *34*, 1679–1682.
- Cooper, R. F., and D. L. Kohlstedt (1984), Solution-precipitation enhanced diffusional creep of partially molten olivine-basalt aggregates during hot pressing, *Tectonophysics*, *107*, 207–233.
- Dimanov, A., G. Dresen, and R. Wirth (2000), The effect of melt distribution on the rheology of plagioclase rocks, *Tectonophysics*, *328*, 307–327.
- Drury, M. R., and J. D. Fitz Gerald (1998), Mantle rheology: Insights from laboratory studies of deformation and phase transition, in *The Earth's Mantle, Composition, Structure and Evolution*, edited by I. Jackson, pp. 503–560, Cambridge Univ. Press, New York.
- Farver, J. R., and R. A. Yund (2000), Silicon diffusion in forsterite aggregates: Implications for diffusion accommodated creep, *Geophys. Res. Lett.*, *27*, 2337–2340.
- Faul, U. H., and D. Scott (2006), Grain growth in partially molten olivine, *Contrib. Mineral. Petrol.*, *151*, 101–111, doi:10.1007/s00410-005-0048-1.
- Faul, U. H., J. D. Fitz Gerald, and I. Jackson (2004), Shear wave attenuation and dispersion in melt-bearing olivine polycrystals: 2. Microstructural interpretation and seismological implications, *J. Geophys. Res.*, *109*, B06202, doi:10.1029/2003JB002407.
- Fitz Gerald, J. D., and P. N. Chopra (1982), Deformation mechanisms in dunite—The results of high temperature testing, in *Proc. Sixth Intl. Conf. Strength Metals and Alloys*, edited by R. C. Gifkins, Elsevier, New York.
- Frey, F. A., and M. Prinz (1978), Ultramafic inclusions from San Carlos, Arizona: Petrologic and geochemical data bearing on their petrogenesis, *Earth Planet. Sci. Lett.*, *38*, 129–176.
- Frost, H. J., and M. F. Ashby (1982), *Deformation-Mechanism Maps, The Plasticity of Metals and Ceramics*, Elsevier, New York.
- Green, D. H., and T. J. Falloon (1998), Pyrolyte: A Ringwood concept and its current expression, in *The Earth's Mantle, Composition, Structure and Evolution*, edited by I. Jackson, chap. 7, pp. 311–378, Cambridge Univ. Press, New York.
- Hirth, G., and D. L. Kohlstedt (1995), Experimental constraints on the dynamics of the partially molten upper mantle: Deformation in the diffusion creep regime, *J. Geophys. Res.*, *100*, 1981–2001.
- Hirth, G., and D. L. Kohlstedt (1996), Water in the oceanic upper mantle: Implications for rheology, melt extraction and the evolution of the lithosphere, *Earth Planet. Sci. Lett.*, *144*, 93–108.
- Hirth, G., and D. L. Kohlstedt (2003), *Inside the Subduction Factory, Geophysical Monograph*, vol. 138, Rheology of the upper mantle and the mantle wedge: A view from the experimentalists, pp. 83–105, AGU, Washington, D. C.
- Jackson, I. (2000), Laboratory measurement of seismic wave dispersion and attenuation: Recent progress, in *Earth's Deep Interior: Mineral Physics and Tomography From the Atomic to the Global Scale, Geophysical Monograph*, vol. 117, edited by S. I. Karato, A. M. Forte, R. C. Liebermann, G. Masters, and L. Stixrude, pp. 265–289, AGU, Washington, D. C.
- Jackson, I., D. Fitz Gerald, and H. Kokkonen (2000), High-temperature viscoelastic relaxation in iron and its implications for the shear modulus and attenuation in the Earth's inner core, *J. Geophys. Res.*, *105*, 23,605–23,634.
- Jackson, I., J. D. Fitz Gerald, U. H. Faul, and B. H. Tan (2002), Grain-size-sensitive seismic wave attenuation in polycrystalline olivine, *J. Geophys. Res.*, *107*(B12), 2360, doi:10.1029/2001JB001225.
- Jackson, I., U. H. Faul, J. Fitz Gerald, and B. H. Tan (2004), Shear wave attenuation and dispersion in melt-bearing olivine polycrystals: 1. Specimen fabrication and mechanical testing, *J. Geophys. Res.*, *109*, B06201, doi:10.1029/2003JB002406.
- Ji, S., Z. Wang, and R. Wirth (2001), Bulk flow strength of forsterite-enstatite composites as a function of forsterite content, *Tectonophysics*, *341*, 69–93.
- Karato, S. I. (1989), Grain growth kinetics in olivine aggregates, *Tectonophysics*, *168*, 255–273.
- Karato, S. I., M. S. Paterson, and J. D. Fitz Gerald (1986), Rheology of synthetic olivine aggregates: Influence of grain size and water, *J. Geophys. Res.*, *91*, 8151–8176.
- McDonnell, R. D., C. J. Peach, and C. J. Spiers (1999), Flow behaviour of fine-grained synthetic dunite in the presence of 0.5 wt% H<sub>2</sub>O, *J. Geophys. Res.*, *104*, 17,823–17,845.
- Mei, S., and D. L. Kohlstedt (2000a), Influence of water on plastic deformation of olivine aggregates: 1. Diffusion creep regime, *J. Geophys. Res.*, *105*, 21,457–21,469.
- Mei, S., and D. L. Kohlstedt (2000b), Influence of water on plastic deformation of olivine aggregates: 2. Dislocation creep regime, *J. Geophys. Res.*, *105*, 21,471–21,481.
- Nichols, S. J., and S. J. Mackwell (1991), Grain growth in porous olivine aggregates, *Phys. Chem. Miner.*, *18*, 269–278.
- Paterson, M. S. (1990), Rock deformation experimentation, in *The Brittle-Ductile Transition in Rocks, Geophys. Monogr. Ser.*, vol. 56, edited by A. G. Duba, pp. 187–194, AGU, Washington, D. C.

- Poirier, J. P. (1985), *Creep of Crystals—High-Temperature Deformation Processes in Metals, Ceramics and Minerals*, Cambridge Univ. Press, New York.
- Ranalli, G. (1995), *Rheology of the Earth*, 2nd ed., CRC Press, Boca Raton, Fla.
- van der Waal, D., P. N. Chopra, M. R. Drury, and J. D. Fitz Gerald (1994), Relationships between dynamically recrystallized grain size and deformation conditions in experimentally deformed olivine rocks, *Geophys. Res. Lett.*, *20*, 1479–1482.
- Wirth, R. (1996), Thin amorphous films 1–2 nm at olivine grain boundaries in mantle xenoliths from San Carlos, Arizona, *Contrib. Mineral. Petrol.*, *124*, 44–54.
- Zimmerman, M. E., and D. L. Kohlstedt (2004), Rheological properties of partially molten lherzolite, *J. Petrol.*, *45*, 275–298.
- 
- U. H. Faul, Department of Earth Sciences, Boston University, 675 Commonwealth Avenue, Boston, MA 02215, USA. (ufaul@bu.edu)
- I. Jackson, Research School of Earth Sciences, The Australian National University, Canberra 0200, Australia.